Level Set Image Segmentation with a Statistical Overlap Constraint

Ismail Ben Ayed[1], Shuo Li[1], and Ian Ross[2]

[1] GE Healthcare, London, ON, Canada
[2] London Health Sciences Centre, London, ON, Canada

Abstract. This study investigates active curve image segmentation with a *statistical overlap constraint*, which biases the overlap between the non-parametric (kernel-based) distributions of image data within the segmentation regions–a foreground and a background–to a statistical description learned *a priori*. We model the overlap, measured via the Bhattacharyya coefficient, with a Gaussian prior whose parameters are estimated from a set of relevant training images. This can be viewed as a generalization of current intensity-driven constraints for difficult situations where a significant overlap exists between the distributions of the segmentation regions. We propose to minimize a functional containing the overlap constraint and classic regularization terms, compute the corresponding Euler-Lagrange curve evolution equation, and give a simple interpretation of how the statistical overlap constraint influences such evolution. A representative number of statistical, quantitative, and comparative experiments with Magnetic Resonance (MR) cardiac images and Computed Tomography (CT) liver images demonstrate the desirable properties of the statistical overlap constraint. First, it outperforms significantly the likelihood prior commonly used in level set segmentation. Second, it is *easy-to-learn*; we demonstrate experimentally that the Gaussian assumption is sufficient for cardiac images. Third, it can relax the need of both complex geometric training and accurate learning of the background distribution, thereby allowing more flexibility in clinical use.

1 Introduction

Image segmentation is a fundamental task in medical image analysis [2]–[9], [23]–[25]. It consists of partitioning an image into two regions: a target object (foreground), for instance a specific organ, and a background. Level set functional minimization, which uses an active curve to delineate the target object, has resulted in the most effective and flexible segmentation algorithms [10]–[20], mainly because it allows introducing a wide range of photometric and geometric constraints on the solution. It has become very popular in medical image analysis [2]–[9], [23]–[25] because there are several applications where anatomical entities can be enclosed within a closed contour. Furthermore, the level set representation of curve evolution extends readily to higher dimensions, and allows to compute easily the geometric characteristics of objects.

J.L. Prince, D.L. Pham, and K.J. Myers (Eds.): IPMI 2009, LNCS 5636, pp. 589–601, 2009.

Level set segmentation consists of evolving a curve to delineate the target object. The curve evolution equation is obtained by optimizing a functional which, generally, contains a data term measuring the conformity of photometric image data (e.g. intensity) within each region to a given statistical description. Chan and Vese [1] pioneered a data term, which measures the conformity of image data within each region to the piecewise constant model. Albeit applicable only to segmentation regions where image data is approximately constant, the Chan-Vese model has established the potential of region-based active contours, and has been widely used in medical image analysis [2]–[5], [7]. More generally, most of segmentation algorithms are stated as a Bayesian inference problem [8]–[14], [21]–[22], [26] where optimization of the data term amounts to maximizing the *likelihood* of the image. This corresponds to maximizing the conditional probability of pixel data given the assumed model distributions within the object and background. The way of estimating model distributions divides segmentation methods into two categories: unsupervised methods, where model distributions are estimated from the current image along with the segmentation process, and methods using *likelihood priors*, where model distributions are learned *a priori*[1] from a set of segmented training images [8], [9], or interactively from user-specified pixels [21]–[22]. Embedding likelihood priors in image segmentation has significantly improved the performances of unsupervised methods [10]. It has led to promising results in medical image segmentation [8], [9], [21]. Unfortunately, likelihood priors require both object and background models. This can be a limitation in medical image analysis because, within a class of images depicting the same object, the background distribution generally undergoes high variations and, therefore, is difficult to learn. More importantly, they can not incorporate information about the *overlap* between the distributions of image data within the object and background–they measure only pixelwise information and, as such, are not sufficient to segment images where a significant overlap (or similarity) exists between the actual distributions within the foreground and background (cf. the typical example in Fig. 1). Recent studies have shown the advantages and effectiveness of using *distributions measures* in object tracking [18]–[20] and image segmentation [15]–[17]. In the context of image segmentation, curve evolution is derived so that, at convergence, the final curve minimizes the overlap (or similarity) between the photometric distributions of the foreground and background regions [15]–[17].

Whether based the likelihood principle or distribution measures, existing segmentation methods assume, implicitly or explicitly, that the overlap between the distributions of image data within the object and its background has to be minimal. The assumption of minimal overlap may not be valid in many applications in medical image analysis where segmentation is often complicated by the similarity in photometric properties between the segmentation regions (cf. the

[1] For instance, segmenting a class of images depicting the same organ and having similar photometric patterns is common in medical image analysis [8]. In this case, learning model distributions from segmented training images is very useful.

typical example in Fig. 1). In this case, adding complex training-based geometric[2] constraints to existing photometric constraints was inevitable to prevent curve spilling and obtain satisfying results [5], [7], [8].

This study investigates image segmentation with a *statistical overlap constraint*, which biases the overlap between the distributions of photometric data within the segmentation regions to a statistical description learned *a priori*. We model the overlap, measured via the Bhattacharyya coefficient, with a Gaussian prior whose parameters are estimated from a set of relevant training images. The overlap constraint can be viewed as a *generalization* of current intensity-driven constraints for difficult situations where a significant overlap exists between the intensity distributions of the foreground and background regions (cf. the typical example in Fig. 1). Used in conjunction with classic regularization terms, the statistical overlap constraint is minimized by curve evolution via the Euler-Lagrange equation. A quantitative and comparative performance evaluation over a representative number of experiments with Magnetic Resonance (MR) cardiac images and Computed Tomography (CT) liver images demonstrate that the proposed constraint outperforms significantly the likelihood prior commonly used in image segmentation. Furthermore, it is *easy-to-learn*; we demonstrate experimentally that the overlap between the intensity distributions within the heart myocardium and the background in cardiac images can be modeled accurately with the Gaussian distribution (cf. Fig. 2 a and b). The proposed method can relax, on one hand, the need of complex geometric constraints and, on the other hand, accurate learning of the background distribution, thereby leading to more flexibility in clinical use.

2 The Proposed Statistical Overlap Constraint

Let $I_{\mathbf{x}} = I(\mathbf{x}) : \Omega \subset \mathbb{R}^2 \rightarrow \mathcal{Z} \subset \mathbb{R}$ be an image function from the domain Ω to the space $\mathcal{Z}$ of photometric variables. Let $\boldsymbol{\Gamma}(s) : [0,1] \rightarrow \Omega$ be a closed planar parametric curve. The purpose of this study is to evolve $\boldsymbol{\Gamma}$ in order to divide Ω into two regions: $\mathbf{R}_{in} = \mathbf{R}_{\boldsymbol{\Gamma}}$, corresponding to the interior of $\boldsymbol{\Gamma}$ (foreground), and $\mathbf{R}_{out} = \mathbf{R}_{in}^c = \mathbf{R}_{\boldsymbol{\Gamma}}^c$, corresponding to the exterior of $\boldsymbol{\Gamma}$ (background). The evolution equation of $\boldsymbol{\Gamma}$ is sought by optimizing a statistical overlap constraint. To introduce such constraint, we first consider the following definitions:

- $\mathbf{P}_{out}$ is the nonparametric (kernel-based) estimate of the distribution of image data outside $\boldsymbol{\Gamma}$

$$\forall z \in \mathcal{Z} \quad \mathbf{P}_{out}(z) = \frac{\int_{\mathbf{R}_{out}} K(z - I_{\mathbf{x}}) d\mathbf{x}}{\mathbf{A}_{out}}, \tag{1}$$

where $\mathbf{A}_{out}$ is the area of region $\mathbf{R}_{out}$: $\mathbf{A}_{out} = \int_{\mathbf{R}_{out}} d\mathbf{x}$. Typical choices of K are the Dirac function and the Gaussian kernel [16]: $K(y) = \frac{1}{\sqrt{2\pi h^2}} exp^{-\frac{y^2}{2h^2}}$, where h is the kernel width.

[2] Geometric properties include object shape, spatial position, and inter-object spatial relations.

- $\mathcal{B}(f/g)$ is the Bhattacharyya coefficient measuring the amount of overlap between two statistical samples f and g

$$\mathcal{B}(f/g) = \sum_{z \in \mathcal{Z}} \sqrt{f(z)g(z)} \tag{2}$$

Note that the values of $\mathcal{B}$ are always in $[0, 1]$, where 0 indicates that there is no overlap, and 1 indicates a perfect match.

We assume that the foreground region, i.e., the target object to be segmented, is characterized by a model distribution, $\mathcal{M}_{in}$, which can be learned over a set of training images and segmentation examples. Consider the following measure of *overlap* between the sample distribution outside the curve (background) and the model distribution of the object (foreground)

$$\mathcal{O}(\boldsymbol{\Gamma}, \mathcal{M}_{in}) = \mathcal{B}(\mathbf{P}_{out}/\mathcal{M}_{in}) = \sum_{z \in \mathcal{Z}} \sqrt{\mathbf{P}_{out}(z)\mathcal{M}_{in}(z)} \tag{3}$$

In order to incorporate prior statistical information about the photometric similarities between the object and the background, we assume that $\mathcal{O}(\boldsymbol{\Gamma}, \mathcal{M}_{in})$ is a random variable following a Gaussian distribution

$$\mathcal{N}\left(\mathcal{O}(\boldsymbol{\Gamma}, \mathcal{M}_{in}), \mu, \sigma\right) = \frac{1}{\sqrt{2\pi\sigma^2}} exp^{-\frac{(\mathcal{O}(\boldsymbol{\Gamma}, \mathcal{M}_{in}) - \mu)^2}{2\sigma^2}} \tag{4}$$

Parameters μ and σ are learned beforehand over a set of relevant segmented training images different from the test images (images of interest). Parametric distributions other than the Gaussian distribution can be employed to model the overlap prior. This would change the final curve evolution equation, but would not change the method *conceptually*. We will show in the experiments that the Gaussian assumption is sufficient in many practical cases in medical image analysis. For instance, the overlap between the intensity distributions within the heart myocardium and the background in Magnetic Resonance Images (MRI) can be modeled accurately with the Gaussian distribution (refer to Fig. 2 b).

We propose to minimize with respect to $\boldsymbol{\Gamma}$ a *statistical overlap term* which measures the conformity of $\mathcal{O}(\boldsymbol{\Gamma}, \mathcal{M}_{in})$ to a Gaussian model described by μ and σ

$$\mathcal{F}\left(\mathcal{O}(\boldsymbol{\Gamma}, \mathcal{M}_{in}), \mu, \sigma\right) = \sqrt{-\log\ \mathcal{N}\left(\mathcal{O}(\boldsymbol{\Gamma}, \mathcal{M}_{in}), \mu, \sigma\right)} \tag{5}$$

The *statistical overlap* term can be viewed as a *generalization* of the *distribution-based* terms proposed recently for image segmentation [15], [16], [17], and object tracking [18], [19], [20]. The particular case corresponding to $\mu = 0$ is an *explicit* form of assuming that the overlap between the intensity distributions of the object and background is *minimal*. Such assumption is *implicit* in existing level set segmentation methods. The proposed overlap term is more *versatile* than existing data terms. It addresses cases in which a significant overlap (cf. the typical example in Fig. 1) exists between the intensity distributions within the object and background and, as such, the ensuing algorithm is more widely applicable than existing level set segmentation algorithms.

We propose to minimize an active curve segmentation functional containing the proposed statistical overlap term and classic regularization terms [1], namely, the length of curve $\boldsymbol{\Gamma}$ and the area of the region within $\boldsymbol{\Gamma}$

$$\mathcal{E}_{\mathbf{O}} = \lambda \mathcal{F}\left(\mathcal{O}(\boldsymbol{\Gamma}, \mathcal{M}_{in}), \mu, \sigma\right) + \alpha \oint_{\boldsymbol{\Gamma}} ds + \nu \int_{\mathbf{R}_{in}} d\mathbf{x}, \tag{6}$$

where λ, α, and ν are positive constants to weigh the contribution of each constraint.

3 Minimization Equation via Curve Evolution

The curve evolution equation is obtained by minimizing $\mathcal{E}_{\mathbf{O}}$ with respect to $\boldsymbol{\Gamma}$. To this end, we derive the *Euler-Lagrange* gradient descent equation by embedding curve $\boldsymbol{\Gamma}$ in a one-parameter family of curves: $\boldsymbol{\Gamma}(s,t) : [0,1] \times \mathbb{R}_+ \rightarrow \Omega$, and solving the partial differential equation:

$$\frac{\partial \boldsymbol{\Gamma}}{\partial t} = -\frac{\partial \mathcal{E}_{\mathbf{O}}}{\partial \boldsymbol{\Gamma}} = -\lambda \frac{\partial \mathcal{F}\left(\mathcal{O}(\boldsymbol{\Gamma}, \mathcal{M}_{in}), \mu, \sigma\right)}{\partial \boldsymbol{\Gamma}} - \alpha \frac{\partial \oint_{\boldsymbol{\Gamma}} ds}{\partial \boldsymbol{\Gamma}} - \nu \frac{\partial \int_{\mathbf{R}_{in}} d\mathbf{x}}{\partial \boldsymbol{\Gamma}}, \tag{7}$$

where t is an artificial time parameterizing the descent direction, and $\frac{\partial \mathcal{E}_{\mathbf{O}}}{\partial \boldsymbol{\Gamma}}$ denotes the functional derivative of $\mathcal{E}_{\mathbf{O}}$ with respect to $\boldsymbol{\Gamma}$.

To derive the final curve evolution equation, we need to compute the functional derivative of the statistical overlap term with respect to $\boldsymbol{\Gamma}$. We have

$$\frac{\partial \mathcal{F}\left(\mathcal{O}(\boldsymbol{\Gamma}, \mathcal{M}_{in}), \mu, \sigma\right)}{\partial \boldsymbol{\Gamma}} = \frac{\left(\mathcal{O}(\boldsymbol{\Gamma}, \mathcal{M}_{in}) - \mu\right)}{2\sigma^2 \, \mathcal{F}\left(\mathcal{O}(\boldsymbol{\Gamma}, \mathcal{M}_{in}), \mu, \sigma\right)} \frac{\partial \mathcal{O}(\boldsymbol{\Gamma}, \mathcal{M}_{in})}{\partial \boldsymbol{\Gamma}} \tag{8}$$

Now we need to compute $\frac{\partial \mathcal{O}(\boldsymbol{\Gamma}, \mathcal{M}_{in})}{\partial \boldsymbol{\Gamma}}$ in (8). We have

$$\frac{\partial \mathcal{O}(\boldsymbol{\Gamma}, \mathcal{M}_{in})}{\partial \boldsymbol{\Gamma}} = \frac{1}{2} \int_{z \in \mathcal{Z}} \sqrt{\frac{\mathcal{M}_{in}(z)}{\mathbf{P}_{out}(z)}} \frac{\partial \mathbf{P}_{out}(z)}{\partial \boldsymbol{\Gamma}} \tag{9}$$

To derive the final expression of $\frac{\partial \mathcal{O}(\boldsymbol{\Gamma}, \mathcal{M}_{in})}{\partial \boldsymbol{\Gamma}}$, we need to compute $\frac{\partial \mathbf{P}_{out}(z)}{\partial \boldsymbol{\Gamma}}$. To this end, we use the result in [26], which shows that for a scalar function g and a curve $\boldsymbol{\Gamma}$, the functional derivative with respect to $\boldsymbol{\Gamma}$ of the integral of g over the region outside $\boldsymbol{\Gamma}$, i.e., $\mathbf{R}^c_{\boldsymbol{\Gamma}}$=$\mathbf{R}_{out}$, is given by $\frac{\partial \int_{\mathbf{R}_{out}} g(\mathbf{x}) d\mathbf{x}}{\partial \boldsymbol{\Gamma}(s,t)} = -g\left(\boldsymbol{\Gamma}(s,t)\right) \boldsymbol{n}(s,t)$, where $\boldsymbol{n}(s,t)$ is the outward unit normal to $\boldsymbol{\Gamma}$ at (s,t). Applying this proposition to $\mathbf{A}_{out}$ and $\int_{\mathbf{R}_{out}} K(z - I_{\mathbf{x}}) d\mathbf{x}$ in $\frac{\partial \mathbf{P}_{out}(z)}{\partial \boldsymbol{\Gamma}}$ yields, after some algebraic manipulations

$$\frac{\partial \mathbf{P}_{out}(z)}{\partial \boldsymbol{\Gamma}(s,t)} = \frac{1}{\mathbf{A}_{out}} \big(\mathbf{P}_{out}(I_{\boldsymbol{\Gamma}(s,t)}) - K(z - I_{\boldsymbol{\Gamma}(s,t)})\big) \boldsymbol{n}(s,t) \tag{10}$$

Embedding (10) into (9), and after some algebraic manipulations, we obtain:

$$\frac{\partial \mathcal{O}(\boldsymbol{\Gamma}, \mathcal{M}_{in})}{\partial \boldsymbol{\Gamma}(s,t)} = \frac{1}{2\mathbf{A}_{out}} \left(\mathcal{O}(\boldsymbol{\Gamma}, \mathcal{M}_{in}) - \int_{z \in \mathcal{Z}} K(z - I_{\boldsymbol{\Gamma}(s,t)}) \sqrt{\frac{\mathcal{M}_{in}(z)}{\mathbf{P}_{out}(z)}} dz \right) \boldsymbol{n}(s,t) \tag{11}$$

Using (11) and the classic derivative of the regularization terms [1] in (8) gives the final curve evolution equation:

$$\frac{\partial \boldsymbol{\Gamma}(s,t)}{\partial t} = \{ \underbrace{\frac{(\mathcal{O}(\boldsymbol{\Gamma},\mathcal{M}_{in})-\mu)}{2\sigma^2 \mathcal{F}\left(\mathcal{O}(\boldsymbol{\Gamma},\mathcal{M}_{in}),\mu,\sigma\right)}}_{Overlap\ constraint\ influence} \underbrace{\frac{\lambda}{2\mathbf{A}_{out}}\left(\int_{z\in\mathcal{Z}} K(z-I_{\boldsymbol{\Gamma}(s,t)})\sqrt{\frac{\mathcal{M}_{in}(z)}{\mathbf{P}_{out}(z)}}dz - \mathcal{O}(\boldsymbol{\Gamma},\mathcal{M}_{in})\right)}_{Flow\ optimizing\ the\ overlap\ measure\ \mathcal{O}(\boldsymbol{\Gamma},\mathcal{M}_{in})} + \alpha\kappa(s,t) - \nu\}\boldsymbol{n}(s,t), \tag{12}$$

where $\kappa(s,t)$ is the mean curvature function of $\boldsymbol{\Gamma}$. Note that $\mathcal{O}(\boldsymbol{\Gamma},\mathcal{M}_{in})$, $\mathbf{P}_{out}$, and $\mathbf{A}_{out}$ depend on the curve and, consequently, *need to be updated along with the evolution process*. The level-set framework [27] is used to implement the evolution equation in (12). Level sets have well-known advantages over explicit curve discretization and can be effected by stable numerical schemes [27].

Interpretation: Let us give an interpretation of how the overlap constraint guides the curve. The learned mean μ influences the sign of the multiplicative coefficient (*overlap constraint influence*) affected to the flow optimizing the overlap measure $\mathcal{O}(\boldsymbol{\Gamma},\mathcal{M}_{in})$, i.e., $\frac{\partial \mathcal{O}(\boldsymbol{\Gamma},\mathcal{M}_{in})}{\partial \boldsymbol{\Gamma}}$. This coefficient is *negative* when the overlap $\mathcal{O}(\boldsymbol{\Gamma},\mathcal{M}_{in})$ is *superior* to its most likely value μ. In this case, the overlap constraint results in a curve evolution which *decreases* $\mathcal{O}(\boldsymbol{\Gamma},\mathcal{M}_{in})$. By contrast, when $\mathcal{O}(\boldsymbol{\Gamma},\mathcal{M}_{in})$ is *inferior* to μ, the coefficient becomes *positive* and the curve evolution *increases* $\mathcal{O}(\boldsymbol{\Gamma},\mathcal{M}_{in})$. The overlap constraint leads to a curve evolution which keeps $\mathcal{O}(\boldsymbol{\Gamma},\mathcal{M}_{in})$ close to its most likely value. The learned variance σ affects the weight of the overlap constraint. The smaller σ, the higher such weight. This is intuitive because a small variance σ indicates that μ is a reliable estimation of the overlap and, as such, it gives more importance to the overlap constraint flow. On the contrary, a high variance gives more importance to the other functional terms.

3.1 Experiments

To demonstrates clearly the advantage of using overlap constraint over commonly used likelihood priors [8], [9], [21], [22], we first give a typical example. Then we describe a *quantitative* and *comparative* performance evaluation over a representative number of experiments on cardiac images. Evaluation of the segmentation method we propose, referred to as Overlap Constraint Method (**OCM**), is supported by extensive comparisons with a Likelihood Prior Method (**LPM**). *The same training images, curve initializations, and parameters were used for both methods*. We also demonstrate experimentally that the overlap prior is *easy-to-learn* in an important application, namely segmentation of the Left Ventricle (LV) in cardiac Magnetic Resonance Images (MRI), where the overlap between the intensity distributions within the heart myocardium and the background

can be modeled accurately with a Gaussian distribution. Finally, we show a representative sample of the tests with Computed Tomography (CT) images and cardiac MRI, which illustrates the effectiveness of the proposed method.

Overlap constraint vs. likelihood prior: We first show a typical example of our extensive testing with cardiac MRI. Fig. 1 (a) depicts the expected (manual) segmentations of the LV cavity (region inside the green curve) and the myocardium (ring between the green and blue curves). Fig. 1 (b) illustrates the significant overlap between the intensity distributions of the myocardium, considered as a foreground (or object), and the background. Our purpose is to use

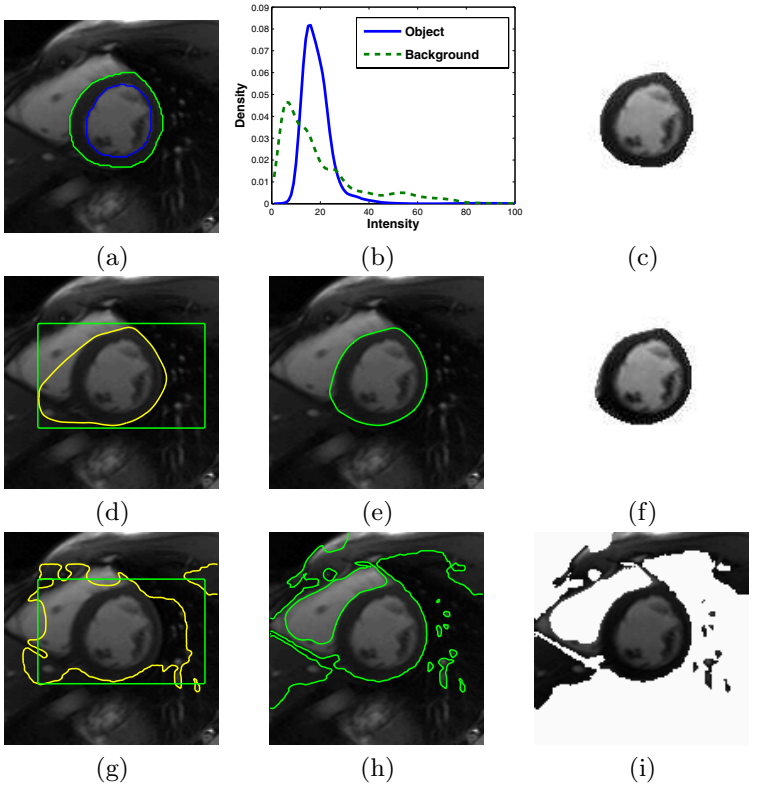

Fig. 1. A typical example of the Left Ventricle (LV) segmentation. First line: (a) expected (manual) delineations of the LV (region inside the green curve) and the myocardium (ring between the green and blue curves); (b) overlap between the intensity distributions of the myocardium and the background (region outside the green curve); (c) manual LV segmentation. Segmentation *with the overlap constraint*, i.e., with **OCM** (second line): (d) initial (green) and intermediate (yellow) curves; (e) curve obtained at convergence; (f) LV segmentation with **OCM**. Segmentation *with the likelihood prior*, i.e., with **LPM** (third line): (g) initial (green) and intermediate (yellow) curves; (h) curve obtained at convergence; (i) LV segmentation with **LPM**. $\mu = 0.72$, $\sigma = 0.037$, $\lambda = 10^3$, $\alpha = 10$, $\nu = 0.1$. *The overlap constraint prevents the curve from spilling.*

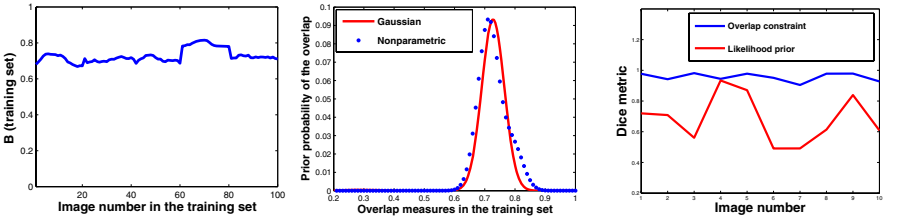

(a) Training (b) Gaussian fit (c) Performance comparisons

Fig. 2. (a)–(b) Training over a set of 100 manually segmented cardiac images (**B** measures the overlap between $\mathcal{M}_{in}$ and the background distribution in manually segmented training images): (a) **B** as a function of the image number; (b) fit between the Gaussian model ($\mu = \mathbf{0}.72$, $\sigma = \mathbf{0}.037$) and the empirical (nonparametric) distribution of the overlap measure **B** in the training set. **(c) Quantitative and comparative performance evaluation**: *Dice Metric* as a function of the test image number for both **OCM** (Overlap constraint) and **LPM** (Likelihood prior). $\lambda = 10^3$, $\alpha = 10$, $\nu = 0.1$.

Table 1. Segmentation accuracy: *Dice measures* of similarity between manual and automatic segmentations. The higher the *Dice metric*, the more accurate the segmentation.

Dice metrics	Mean	Std
Overlap constraint (**OCM**)	0.95	0.026
Likelihood prior (**LPM**)	0.68	0.15

prior information on the overlap between the distributions of the myocardium and the background to automatically detect the interface between them (the green curve), and hence segment the LV depicted in Fig. 1 (c). The latter task is of capital importance in the analysis of cardiac images.

Training: We first proceeded to learning the model distribution of the myocardium, $\mathcal{M}_{in}$, and the parameters of the overlap constraint, μ and σ, over a set of **100** manually segmented training images obtained from **5** different subjects. In Fig. 2 (a), we plotted the measure of overlap between $\mathcal{M}_{in}$ and the background distribution versus the training image number. Such overlap does not vary much and, as shown in Fig. 2 (b), can be modeled accurately with a Gaussian distribution. Our training yielded an overlap mean $\mu = \mathbf{0}.72$ and standard deviation $\sigma = \mathbf{0}.037$. These overlap parameters were used for all our tests on cardiac images. Note that the training images are different from the test images.

Likelihood Prior: The likelihood prior has been commonly used in image segmentation as a data term, such as in [8], [9], [21], [22], and many others. We proceeded to a comparison between the proposed method (**OCM**) and a Likelihood Prior Method (**LPM**) that corresponds to minimizing the following active curve functional:

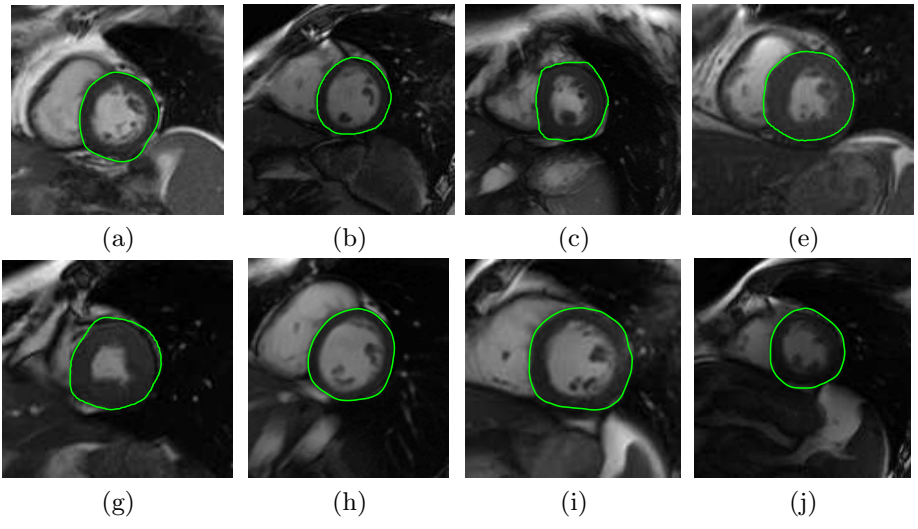

Fig. 3. A representative sample of the tests: height examples of the left ventricle segmentation. $\lambda = 10^3$, $\alpha = 10$, $\nu = 0.1$. The proposed overlap constraint prevents the curves from spilling into the background, which yielded accurate segmentation results, although no additional training-based geometric constraints were used.

$$\mathcal{E}_{\mathbf{L}} = \underbrace{-\lambda \left(\int_{\mathbf{R}_{in}} \log \mathcal{M}_{in}(I_{\mathbf{x}}) d\mathbf{x} + \int_{\mathbf{R}_{out}} \log \mathcal{M}_{out}(I_{\mathbf{x}}) d\mathbf{x} \right)}_{Likelihood\ prior} + \alpha \oint_{\boldsymbol{\Gamma}} ds + \nu \int_{\mathbf{R}_{in}} d\mathbf{x}, \tag{13}$$

i.e., we replaced our overlap constraint in (6) by a commonly used likelihood prior. The latter minimizes minus the image log-likelihood, i.e., maximizes the conditional probability of pixel intensity given the assumed model distributions, $\mathcal{M}_{in}$ and $\mathcal{M}_{out}$, within, respectively, the foreground and background. The same training images, segmentation examples, curve initializations, and weighting parameters were used for both methods (**OCM** and **LPM**). Note that, different from our method, **LPM** needs a prior estimation of the background model distribution $\mathcal{M}_{out}$. For the tests we run with **LPM** for comparisons, we used the actual background distribution, i.e., the correct distribution estimated from a manual segmentation of the current test image. Note that this is advantageous to **LPM** and would not bias our comparative appraisal of the proposed method.

Weighting parameters: The parameters weighting the relative contribution of the intensity terms and the regularization terms were fixed for all the experiments: $\lambda = 10^3$, $\alpha = 10$, $\nu = 0.1$.

Quantitative and comparative evaluation: The typical example in Fig. 1 demonstrates clearly the advantage of using an overlap constraint over a likelihood prior. The third line in Fig. 1 depicts segmentation results with the **LPM**.

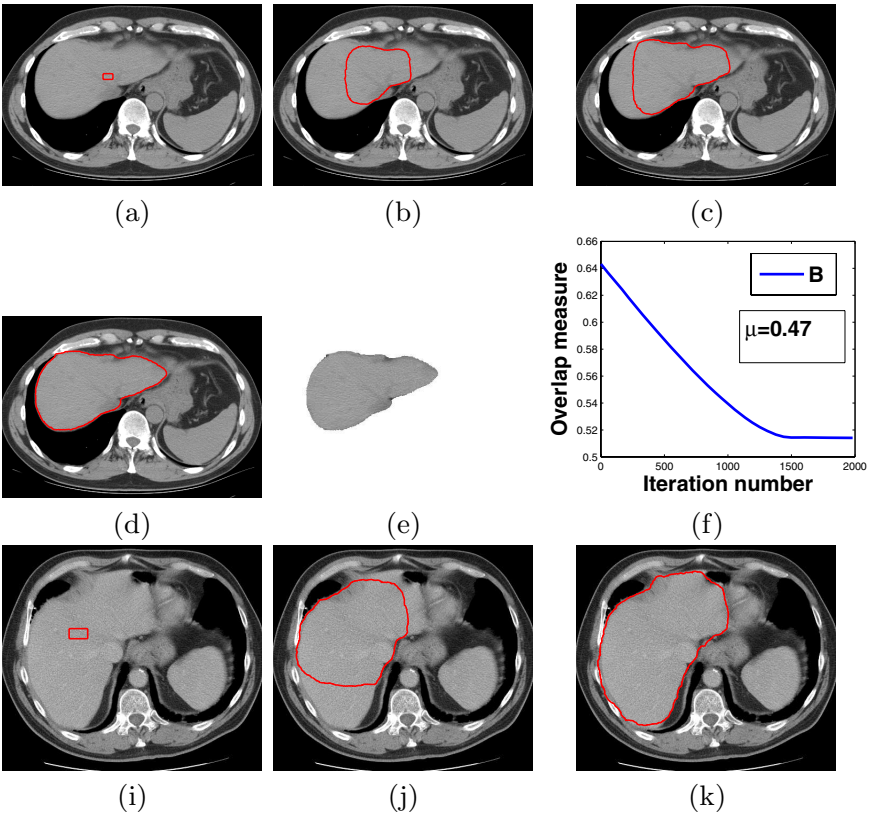

Fig. 4. Liver segmentation. **First example** (a)–(f): (a) initial curve; (b) iteration 400 (intermediate); (c) iteration 800 (intermediate); (d) iteration 1600 (final curve); (e) obtained liver segmentation; (f) evolution of the overlap measure during curve evolution: $\mathbf{B} = \mathcal{O}(\boldsymbol{\Gamma}, \mathcal{M}_{in})$ as a function of the iteration number. Overlap measure obtained at convergence: $\mathbf{B} = \mathbf{0}.51$. **Second example** (i)–(k): (i) initial curve; (j) intermediate curve; (k) final curve. Overlap measure obtained at convergence: $\mathbf{B} = \mathcal{O}(\boldsymbol{\Gamma}, \mathcal{M}_{in}) = \mathbf{0}.50$. Parameters for both examples: $\mu = 0.47$, $\sigma = 0.03$ (μ and σ were learned from 6 images). $\lambda = 10^3$, $\alpha = 10$, $\nu = 0.1$.

Fig. 1 (g) shows initial (green) and intermediate (yellow) curves. The final curve at convergence with the **LPM** is displayed in Fig. 1 (h), and the corresponding left ventricle segmentation in (i). As expected, parts of the background, which have intensity profiles similar to the myocardium, were included inside the final curve. The result with the **LPM** is affected by the significant overlap between the distributions of the myocardium and the background (Fig. 1 (b)). By contrast, the proposed method delineated accurately the left ventricle (Fig. 1 e) and yielded a result (Fig. 1 (f)) which is very similar to the manual segmentation (Fig. 1 (c)). The proposed overlap constraint prevents the curve from spilling

into the background, thereby relaxing the need of complex geometric training. Initial (green) and intermediate (yellow) curves are depicted in (d).

To demonstrate that the overlap constraint is an effective alternative to the likelihood prior, we proceeded to a *quantitative* and *comparative* performance evaluation over a representative number of experiments. We run tests with both **OCM** and **LPM** on **1**0 cardiac MR images obtained from **1**0 different subjects. Performance analysis was carried out by assessing the similarities between automatic segmentations, obtained with both **OCM** and **LPM**, and independent manual segmentations approved by a radiologist. We used the *Dice Metric (DM)* to measure the *similarity* between manual and automatic segmentations. Let $\mathbf{A}_a$, $\mathbf{A}_m$ and $\mathbf{A}_{am}$ be the areas of, respectively, the automatically detected region, the corresponding hand-labeled region and the intersection between them. *DM* is given by $\frac{2\mathbf{A}_{am}}{\mathbf{A}_a+\mathbf{A}_m}$. Area measurements are expressed as the number of pixels within the region. Note that *DM* is always in [0, 1], where *DM* equal to 1 indicates a perfect match between manual and automatic segmentation. Our method yielded a *DM* equal to $\mathbf{0}.95 \pm \mathbf{0}.026$, whereas **LPM** gave a *DM* equal to $\mathbf{0}.68 \pm \mathbf{0}.15$ (refer to table 1). *DM* is expressed as mean $\pm$ standard deviation. Fig. 2 (c) plots the obtained *DM* as a function of the test image number for both **LPM** and **OCM**. The higher *DM*, the more accurate the segmentation result. *Using the same training images, curve initializations, and weighting parameters for both methods, the proposed method (***OCM***) outperforms significantly* **LPM**.

A representative sample of the tests: Here following a representative sample of the results obtained with the proposed method in two challenging segmentation tasks: left ventricle segmentation in MRI and liver segmentation in Computed Tomography (CT) images.

Left ventricle segmentation in MRI: In Fig. 3, we give a representative sample of the tests we run with cardiac images for visual inspection. The green curve represents $\boldsymbol{\Gamma}$ at convergence. The proposed overlap constraint prevents the active curves from spilling into the background, which yielded accurate left ventricle segmentation results, although no additional training-based geometric constraints were used.

Liver segmentation in CT images: Liver segmentation is challenging and has recently attracted research attention [25]. We applied our method to liver segmentation in CT images. The overlap constraint parameters were learned from six training images independent from the test images: $\mu = \mathbf{0}.47$ and $\sigma = \mathbf{0}.03$. Fig. 4 depicts two typical examples. For the first example, initial curve, two intermediate steps, and the curve obtained at convergence are shown, respectively, in Figs. 4 (a), (b), (c), and (d). The obtained liver is depicted in (e). In Fig. 4 (f), we plotted the optimized overlap measure, $\mathbf{B} = \mathcal{O}(\boldsymbol{\Gamma}, \mathcal{M}_{in})$, as a function of the iteration number. At convergence, the obtained overlap measure is equal to $\mathbf{0}.51$, and is close to the learned overlap mean μ. Although parts of the background have intensity profiles similar to the liver, the proposed method yielded an accurate segmentation. The second example of our tests on liver images is depicted in Figs. 4 (i)–(k). Initial curve, one intermediate step, and the curve obtained at convergence are shown, respectively, in Fig. 4 (i), (j), and (k).

The proposed method delineated accurately the liver as visual inspection can show. The overlap measure obtained at convergence is equal to $\mathbf{0}.50$, and is also close to μ. These results demonstrate the effectiveness of the proposed method in various challenging image segmentation tasks.

4 Conclusion

We investigated a statistical overlap constraint for active curve segmentation. This led to an algorithm that relaxes the assumption of minimal overlap and, as such, is more widely applicable than existing level set algorithms. A representative number of statistical, quantitative, and comparative experiments demonstrated the desirable effects of the statistical overlap constraint.

References

1. Chan, T.F., Vese, L.A.: Active Contours without Edges. IEEE Transactions on Image Processing 10(2), 266–277 (2001)
2. Li, C., Huang, R., Ding, Z., Gatenby, C., Metaxas, D.N., Gore, J.C.: A Variational Level Set Approach to Segmentation and Bias Correction of Images with Intensity Inhomogeneity. In: Metaxas, D., Axel, L., Fichtinger, G., Székely, G. (eds.) MICCAI 2008, Part II. LNCS, vol. 5242, pp. 1083–1091. Springer, Heidelberg (2008)
3. Wang, L., Li, C., Sun, Q., Xia, D., Kao, C.-Y.: Brain MR Image Segmentation Using Local and Global Intensity Fitting Active Contours/Surfaces. In: Metaxas, D., Axel, L., Fichtinger, G., Székely, G. (eds.) MICCAI 2008, Part I. LNCS, vol. 5241, pp. 384–392. Springer, Heidelberg (2008)
4. Sun, W., Çetin, M., Chan, R., Reddy, V., Holmvang, G., Chandar, V., Willsky, A.: Segmenting and Tracking the Left Ventricle by Learning the Dynamics in Cardiac Images. In: Christensen, G.E., Sonka, M. (eds.) IPMI 2005. LNCS, vol. 3565, pp. 553–565. Springer, Heidelberg (2005)
5. Kohlberger, T., Cremers, D., Rousson, M., Ramaraj, R., Funka-Lea, G.: 4D Shape Priors for a Level Set Segmentation of the Left Myocardium in SPECT Sequences. In: Larsen, R., Nielsen, M., Sporring, J. (eds.) MICCAI 2006. LNCS, vol. 4190, pp. 92–100. Springer, Heidelberg (2006)
6. Pohl, K.M., Kikinis, R., Wells, W.M.: Active mean fields: Solving the mean field approximation in the level set framework. In: Karssemeijer, N., Lelieveldt, B. (eds.) IPMI 2007. LNCS, vol. 4584, pp. 26–37. Springer, Heidelberg (2007)
7. Tsai, A., Yezzi, A., Wells, W., Tempany, C., Tucker, D., Fan, A., Grimson, W.E., Willsky, A.: A shape-based approach to the segmentation of medical imagery using level sets. IEEE Transactions on Medical Imaging 22(2), 137–154 (2003)
8. Rousson, M., Cremers, D.: Efficient Kernel Density Estimation of Shape and Intensity Priors for Level Set Segmentation. In: Duncan, J.S., Gerig, G. (eds.) MICCAI 2005, Part I. LNCS, vol. 3749, pp. 757–764. Springer, Heidelberg (2005)
9. Paragios, N.: A Variational Approach for the Segmentation of the Left Ventricle in Cardiac Image Analysis. International Journal of Computer Vision 50(3), 345–362 (2002)
10. Cremers, D., Rousson, M., Deriche, R.: A Review of Statistical Approaches to Level Set Segmentation: Integrating Color, Texture, Motion and Shape. International Journal of Computer Vision 62, 249–265 (2007)

11. Ben Ayed, I., Mitiche, A., Belhadj, Z.: Multiregion Level Set Partitioning on Synthetic Aperture Radar Images. IEEE Transactions on Pattern Analysis and Machine Intelligence 27(5), 793–800 (2005)
12. Ben Ayed, I., Mitiche, A., Belhadj, Z.: Polarimetric Image Segmentation via Maximum Likelihood Approximation and Efficient Multiphase Level Sets. IEEE Transactions on Pattern Analysis and Machine Intelligence 28(9), 1493–1500 (2006)
13. Ben Ayed, I., Hennane, N., Mitiche, A.: Unsupervised Variational Image Segmentation/Classification using a Weibull Observation Model. IEEE Transactions on Image Processing 15, 3431–3439 (2006)
14. Rousson, M., Paragios, N.: Prior Knowledge, Level Set Representations and Visual Grouping. International Journal of Computer Vision 76(3), 231–243 (2008)
15. Michailovich, O.V., Rathi, Y., Tannenbaum, A.: Image Segmentation Using Active Contours Driven by the Bhattacharyya Gradient Flow. IEEE Transactions on Image Processing 16(11), 2787–2801 (2007)
16. Georgiou, T., Michailovich, O., Rathi, Y., Malcolm, J., Tannenbaum, A.: Distribution Metrics and Image Segmentation. Linear Algebra and its Applications 425, 663–672 (2007)
17. Kim, J., Fisher III, J.W., Yezzi, A., Cetin, M., Willsky, A.S.: A nonparametric statistical method for image segmentation using information theory and curve evolution. IEEE Transactions on Image processing 14(10), 1486–1502 (2005)
18. Zhang, T., Freedman, D.: Improving performance of distribution tracking through background mismatch. IEEE Transactions on Pattern Analysis and Machine Intelligence 27(2), 282–287 (2005)
19. Ben Ayed, I., Li, S., Ross, I.: Tracking Distributions with an Overlap Prior. In: CVPR, Anchorage, AK (2008)
20. Freedman, D., Zhang, T.: Active contours for tracking distributions. IEEE Transactions on Image Processing 13(4), 518–526 (2004)
21. Boykov, Y., Funka-Lea, G.: Graph Cuts and Efficient N-D Image Segmentation. International Journal of Computer Vision 70(2), 109–131 (2006)
22. Rother, C., Kolmogorov, V., Blake, A.: Grabcut-interactive foreground extraction using iterated graph cuts. In: SIGGRAPH 2004 (2004)
23. Ben Ayed, I., Lu, Y., Li, S., Ross, I.: Left Ventricle Tracking Using Overlap Priors. In: Metaxas, D., Axel, L., Fichtinger, G., Székely, G. (eds.) MICCAI 2008, Part I. LNCS, vol. 5241, pp. 1025–1033. Springer, Heidelberg (2008)
24. Lynch, M., Ghita, O., Whelan, P.F.: Segmentation of the Left Ventricle of the Heart in 3-D+t MRI Data Using an Optimized Nonrigid Temporal Model. IEEE Transactions on Medical Imaging 27(2), 195–203 (2008)
25. Ling, H., Kevin Zhou, S., Zheng, Y., Georgescu, B., Suehling, M., Comaniciu, D.: Hierarchical, Learning-based Automatic Liver Segmentation. In: CVPR, Anchorage, AK (2008)
26. Zhu, S.C., Yuille, A.L.: Region Competition: Unifying Snake/balloon, Region Growing and Bayes/MDL/Energy for multi-band Image Segmentation. IEEE Transactions on Pattern Analysis and Machine Intelligence 18(9), 884–900 (1996)
27. Sethian, J.: Level Set Methods and Fast Marching Methods. Cambridge University Press, Cambridge (1999)